Optica Applicata, Vol. LIV, No. 2, 2024
DOI: 10.37190/oa240207

An ultra-wideband plasmonic reflector based on local resonant bandgap and Bragg bandgap

SAN CHEN[1,*], LIANG FANG[1], JIANQIANG LIU[2], SHAN WU[3]

[1]School of Physics and Electronic Information, and Anhui Province Key Laboratory of Intelligent Computing and Applications, Huaibei Normal University, Huaibei 235000, China

[2]College of Science, Jiujiang University, Jiujiang, 332005, China

[3]Key Laboratory of Functional Materials and Devices for Informatics of Anhui Higher Education Institutes, Fuyang Normal University, Fuyang 236037, China

[*]Corresponding author: chensan@chnu.edu.cn.

Unlike previous reports that utilized periodic modulation of insulation layer thickness or dielectrics, we propose the use of split ring resonators (SRRs) and their arrays to modulate the propagation characteristics of MIM plasmon waveguides. Due to the strong resonance backscattering of SRR, resonance transmission valleys appear in the transmission spectra of MIM waveguides. Changing the size of SRR can achieve continuously adjustable positions of resonance transmission valleys. The introduction of SRRs periodic arrays will result in two bands (bandgaps) with transmission minimum in the transmission spectra. Combining the dependence of the two bandgaps on the array period and the field distribution, the two bandgaps are Bragg bandgaps and local resonance bandgaps, respectively. By modulating the local resonance bandgap, the Bragg bandgap can be tuned. The introduction of local bandgap increases the degree of freedom to modulate the transmission characteristics of MIM waveguides. Combining local resonant bandgap and Bragg bandgap can significantly increase the reflection bandwidth, achieve broadband filtering, and facilitate the miniaturization of waveguide devices.

Keywords: metal-insulator-metal waveguides, SRRs, Bragg bandgap, local resonant bandgap.

1. Introduction

Surface plasmon polariton is an electron density wave existing on the metal surface or interface. According to its propagation characteristics, it can be divided into local modes and propagation modes, which can realize local field enhancement and subwavelength propagation of waves. It is widely used to enhance light matter interaction

(such as strong coupling effect, enhanced Raman, fluorescence, laser, photovoltaic, photocatalysis, sensing and detection, *etc*.) and control light propagation (subwavelength transmission, slow light, nano-focusing, negative refraction, super-resolution imaging, *etc*.). Photoelectronic devices based on surface plasmon polariton, such as optical waveguides, light modulators, light sources, lasers, lenses, sensors and detectors can achieve ultra-small dimensions, ultra low power consumption, ultra sensitivity, and low losses.

Optical waveguides are used for interconnecting optoelectronic devices and realizing communication between them. Although metal plasmon waveguides have significant transmission losses, plasmon waveguides can break through diffraction limits and achieve sub wavelength scale propagation of optical signals, which has potential application prospects in high-density optoelectronic integrated circuits. In recent years, various types of plasmon optical waveguides have been proposed, such as metal nanoparticle chain waveguides [1,2], metallic wire, stripe and slab waveguides [3,4], groove [5-10], wedge waveguides [5-6,11-13], dielectric loaded metal waveguides [14,15], and hybrid plasmon waveguides [16-18]. Metal/insulator/metal (MIM) waveguides can achieve a good balance between propagation length and mode confinement, and this type of waveguide is compatible with mature semiconductor planar microfabrication processes, which can effectively reduce processing costs.

To study the propagation characteristics, modulation, and implementation of specific functions of MIM waveguides, various structures based on MIM waveguides have been proposed. Dionne systematically studied the dispersion, mode characteristics, propagation length, and skin depth of $Ag/SiO_2/Ag$ waveguides, obtaining a field confinement of 20 nm and the propagation length of over 10 μm [19]. Curved waveguides and beam splitters can achieve low loss propagation and beam splitting of waves over a wide frequency range [20-23]. MIM Mach Zehnder interferometer (M-Z interferometer) with different structures is used for optical routing and optical switches [24-26]. SHIN *et al*. used MIM to construct a lens and achieve full angle negative refraction imaging [27]. The systematic and in-depth studies on slow light of MIM waveguides were carried out [28-31]. Atwater research group proved that MIM structure has a slow light effect superior to other structures, and broadband efficient slow light is realized in MIM structure [29]. Bragg reflectors based on MIM waveguide structures have received widespread attention [32-36]. WANG *et al*. proposed metal heterojunction plasmon Bragg reflectors and nanocavities [32]. HOSSEINI and MASSOUD introduced two alternating periodic media in MIM waveguides to obtain low loss plasmon Bragg reflectors [33]. HAN *et al*. designed a periodic modulated Bragg reflector with different MIM waveguide insulator layer thickness [34], which combines MIM insulator layer thickness and dielectric periodic modulation. The high refractive index material is inserted into a narrow slit, while the wide slit has a low refractive index material, so the Bragg band-gap is widened and the high reflectivity in the band-gap is obtained [35,36]. In our previous work, we designed MIM waveguide nanocavities to obtain strong coupling effects between the cavities and artificial atoms [37,38], and introduced nonlinear media to achieve strong coupling switching effects [39].

In previous reports, the Bragg bandgap was obtained and widened by periodically modulating the insulator width of the MIM waveguide or the dielectric material within it. In this work, we propose another approach - introducing SRRs into MIM waveguides and utilizing the coherent scattering of SRRs to obtain Bragg bandgaps. However, unlike previous reports, there is another type of bandgap in the transmission spectrum, which is significantly different from the Bragg bandgap. We found that the band-gap does not depend on the atom period, but rather on the SRR size, *i.e.* the resonance of a single SRR. According to the dependence of the transmission dip position on the SRR array period, and the field distribution, it can be inferred that this band-gap originates from the local resonance bandgap resulting from the resonance of individual atoms. By changing the local resonance of SRRs or the period of SRRs array, the relative positions of the Bragg bandgap and local resonance bandgap can be tuned. When the local resonance bandgap is close to the Bragg bandgap, the reflectance can be enhanced and Bragg reflection bandwidth can be widened. This is attributed to the fact that the closer the Bragg bandgap is to the SRR resonance scattering wavelength, the stronger the backscattering of a single atom. The introduction of local resonant bandgap increases the degree of freedom for modulating MIM waveguides.

2. Results and discussion

In this paper, the MIM waveguide is composed of two semi-infinite two-dimensional metal plates with a slit in the middle. The air layer serves as the insulation core layer, and the two two-dimensional metal plates are metallic silver as shown in Fig. 1. The dielectric constant of silver is characterized by the Drude model:

$$\varepsilon_i(\omega) = \varepsilon_\infty - \frac{\omega_p^2}{\omega^2 + j\gamma\omega}$$

In the equation, ω is the angular frequency of the incident light, ω_p is the plasma oscillation frequency of Ag free electron gas, γ is the electron collision frequency, where $\varepsilon_\infty = 3.7$, $\omega_p = 1.3826 \times 10^{16}$ rad/s, $\gamma = 2.7348 \times 10^{13}$ rad/s [40], and the refractive index of the air layer is approximately 1. We use the finite-difference time-domain method (FDTD) to study the transmission characteristics and field distribution of the structure. To eliminate the influence of coupling between SRRs and their image SRRs on the transmission characteristics of waveguides, and only consider the influence of SRRs array period along the waveguide direction and the coupling between SRRs on the transmission of waveguides, we studied the effect of the insulation layer thickness in the middle of the waveguide on the transmission resonance wavelength of a single SRR, as shown in Fig. 1(b). The red and blue solid curves represent the transmission curves of the waveguide at a width of 480 and 500 nm, respectively. It can be clearly seen from the figure that when the thickness of the insulation layer increases to 480 nm or above, the transmission resonance wavelength of a single SRR tends to a fixed wavelength. At this point, the coupling between the SRR and its image can be ignored, and

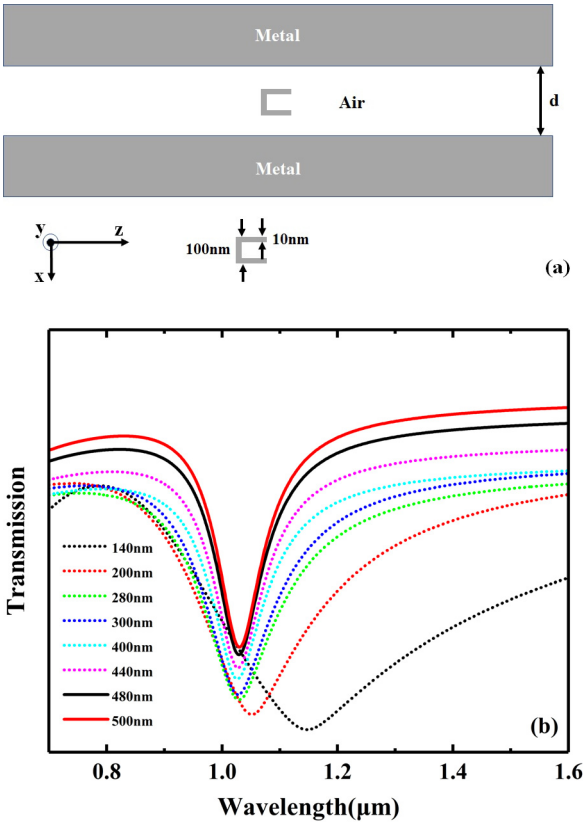

Fig. 1. (a) Schematic illustration of an MIM waveguide with an SRR. The gray region represents silver and the white region represents air layer with thickness *d*. The width of SRR is fixed at 100 nm, its arm length is adjustable, and the width of the Ag strip is 10 nm; (b) The dependence of transmission resonances of the MIM waveguide with an embedded SRR on the insulator layer of thickness *d*.

this fixed wavelength is the resonance wavelength of a single SRR. Therefore, in this work, we fixed the thickness of the insulating medium in the middle of the MIM waveguide at 500 nm. From the figure, we also find that with the increase of waveguide core width, the resonant transmissivity and the resonant Q factor increase, and the transmission resonance changes from the asymmetric Fano profile to the symmetric Lorentzian profile.

Figure 2 shows the dependence of the resonance wavelength of the single SRR on its size-arm length. The geometric dimensions of the U-shaped SRR are shown in Fig. 1, with the arm length of 100 nm and an Ag strip width of 10 nm. Therefore, the length size along the arm direction is 10 nm plus the arm length l. The transmission spectrum of SRR with arm length gradually increasing from 40 to 200 nm was calculated, as shown in Fig. 2(a). It can be clearly seen from the transmission spectra that as the arm length increases, the resonance wavelength of SRR shifts towards the longer wavelength. The dependence of resonance wavelength on the arm length is fitted as

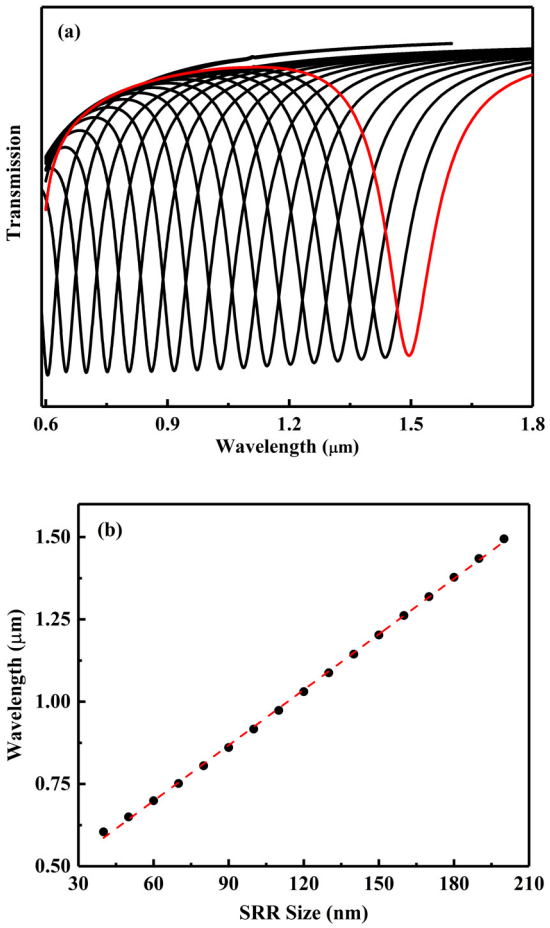

Fig. 2. The dependence of transmission resonances of the MIM waveguide on embedded SRR sizes. (a) The transmission spectra of the MIM waveguide with an embedded SRR with various sizes; (b) The fitted relationship between transmission resonance wavelength and SRR size.

shown in Fig. 2(b), and the resonance wavelength is linearly related to the arm length. From the transmission spectra, it was also found that the transmittance at the resonance wavelength decreases with the decrease of the resonance wavelength, which is due to an increase in Ag loss at the short wavelength side.

In previous reports, broadband high reflection has been achieved by periodically modulating the air core layer thickness of MIM waveguides or introducing periodic media in MIM waveguides. To enhance reflection and improve reflection bandwidth, SRRs periodic arrays are introduced into the waveguide. The thickness of the air core layer in the MIM waveguide remains fixed at 500 nm, and the size of SRRs in the array is 110 × 100 nm and remains fixed as shown in Fig. 3(a), corresponding to a resonance wavelength of 0.92 μm for the SRR. We study the impact of the periodicity of the array on MIM transmission. Figure 3(b) shows the transmission spectra of the waveguides

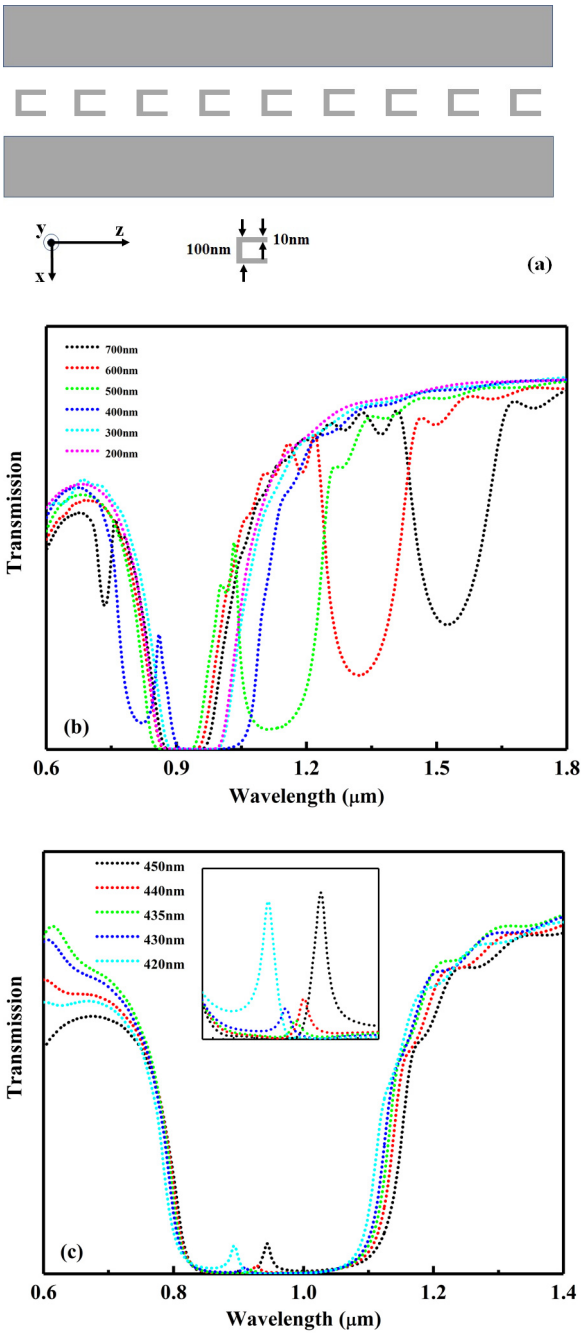

Fig. 3. (a) Schematic illustration of an MIM waveguide with an embedded SRRs array. (b) The dependence of two transmission valleys of the MIM waveguide on SRRs array periods. (c) The transmission spectra with two valleys approaching each other, with the interval between two valleys zoomed in shown in the inset.

with different array periods. It is clearly seen from the figure that there are two transmission valleys. As the array period is gradually shortened from 700 to 200 nm, the transmission valley at the long wavelength shifts towards short wavelengths, which is significantly dependent on the period. Moreover, as the period is shortened, the transmittance decreases and the bandwidth of the transmission valley increases. Compared to the transmission valley on the long wavelength side, the transmission valley on the short wavelength side has lower transmittance. When the period is large, the position of the transmission valley does not change with the shortening of the period. As the period is shortened from 700 to 500 nm, the long wavelength transmission valley gradually approaches the short wavelength transmission valley, and the short wavelength transmission valley undergoes a smaller blueshift. When the array period is 400 nm, the lower transmissivity valley suddenly undergoes a large redshift, with the higher transmissivity valley shifting to the left side of the lower transmissivity valley. As the period is further shortened, the higher transmissivity valley shifts towards the short wavelength and moves out of the window of interest, leaving only a lower transmissivity valley. In order to understand the sudden redshift at the period of 400 nm, we finely tuned the period of the array, which helps to understand the evolution behavior of the two transmission valleys at the closest point, as shown in Fig. 3(c). When the array period gradually decreases from 450 to 435 nm, we can clearly distinguish between the lower transmissivity valley and the higher transmissivity valley. At 435 nm, we cannot distinguish between two transmission valleys based on the higher and lower transmissivity. The difference is that the bandwidth of the two transmission valleys is different. Further reducing the array period increases the difference in transmissivity between the two transmission valleys, and the higher transmissivity valley further deviates from the resonance wavelength of the SRR. In the calculation, we also found that the two transmission valleys cannot overlap, and the two transmission valleys exhibit the repulsive behavior.

To understand the mechanism of the formation of two transmission valleys, we numerically calculated the field distribution with the SRR array period at 600 nm, as shown in Fig. 4. Magnetic field distribution $|H_y|$ at $\lambda = 0.9$ μm, 1.16 μm, 1.32 μm, which locate at the low transmission valley, the high transmission band between the two valleys, and the high transmission valley. The magnetic field distribution at $\lambda = 1.32$ μm exhibits a periodic interference pattern, and the magnetic field amplitude gradually decays along the propagation direction of the wave, which is attributed to the Bragg scattering of the SRR array. Therefore, this transmission valley corresponds to the Bragg bandgap of the corresponding structure. At $\lambda = 1.16$ μm, the magnetic field also exhibits a periodic interference pattern, but there is no obvious attenuation phenomenon, and waves can propagate without attenuation in the structure. What is significantly different from the previous field distribution is that at $\lambda = 0.9$ μm, the magnetic field does not exhibit periodic interference patterns. The magnetic field is mainly localized at the position of SRRs, and the electromagnetic field resonates strongly with each SRR, generating strong resonance scattering. The electromagnetic energy is partially backscattered, and partially localized in the SRR. The first three SRRs are sufficient to generate

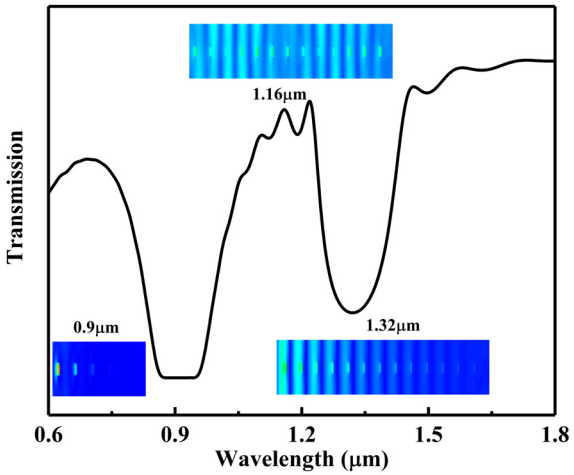

Fig. 4. The transmission spectrum of the MIM waveguide with an embedded atom array period 600 nm. The three insets show the $|H_y|$ field distribution at λ = 0.9 μm, 1.16 μm, 1.32 μm.

strong backscattering, resulting in faster attenuation of the magnetic field along the propagation direction. Considering that this transmission valley does not depend on the array period, it corresponds to a local resonant bandgap [41].

We fix the SRR array period and the SRR size at 600 nm and100 × 100 nm, respectively. The insulator layer width of the MIM waveguide is gradually changed from 550 to 150 nm, and the transmission spectra are shown in Fig. 5. From the figure, it can be seen that as the width decreases, the bandwidth of the Bragg bandgap gradually

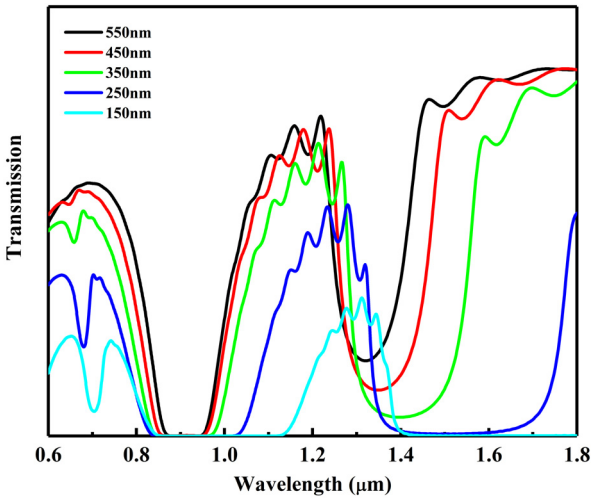

Fig. 5. The dependence of two transmission valleys of the MIM waveguide on its insulator core thickness with fixed SRR array period and SRR sizes.

broadens, and there is a significant red shift and transmittance decrease. The red shift of the Bragg bandgap is attributed to the increasing of the effective refractive index of the MIM waveguide with the decrease of waveguide insulator layer width. Similarly, as the waveguide insulator layer width decreases, the local resonant bandgap exhibits behaviors similar to the Bragg bandgap. The difference is that the redshift and broadening of the local resonant bandgap are mainly attributed to the enhanced coupling effect between SRRs and their images as the waveguide insulator layer width decreases. Comparing the two bandgaps, it can also be found that when the MIM waveguide width is large, the Bragg bandgap is more sensitive to the waveguide width than the local resonant bandgap.

3. Conclusions

In this work, we investigated the modulation of the propagation characteristics of MIM plasmon waveguides by split ring resonators and their arrays. Due to the resonance backscattering of a single SRR, a resonance transmission valley appears in the transmission spectrum of the MIM waveguide, and the resonance wavelength exhibits a linear relationship with the arm length of the SRR. By changing the thickness of the waveguide insulator core layer and utilizing the coupling with the image SRRs, the position of the resonance transmission valley can be made continuously adjustable. Introducing the SRR periodic array into the waveguide, selecting the appropriate SRR size and period will result in two bands (bandgaps) with transmission minimum appearing in the transmission spectrum. By changing the period of the SRR array, it was found that one of the bandgaps moves towards the short wavelength with decreasing of the period, while the other bandgap does not change with the period. Combined with the field distribution, one of them comes from the Bragg bandgap, which is significantly dependent on the array period, while the other comes from a local resonant bandgap, independent of the period. The study also found that as the Bragg bandgap gradually approaches the local resonance bandgap, the transmissivity corresponding to the Bragg bandgap gradually decreases, due to the enhanced backscattering of SRRs at the Bragg bandgap. Changing the thickness of the waveguide insulation core layer can also achieve continuous and adjustable bandgap widths and positions. By utilizing the strong local resonance backscatter of SRRs, lower transmissivity can be achieved with fewer SRRs, which is conducive to the miniaturization of waveguide filtering devices. The introduction of local bandgap increases the degrees of freedom to tune the transmission characteristics of MIM waveguides, and the combination of both the Bragg bandgap and the local resonance bandgap can significantly increase the reflection bandwidth and achieve broadband filtering.

Declarations

Competing interests
The authors declare that they have no known competing financial interests or personal relationships that could have appeared to influence the work reported in this paper.

Author contribution
San Chen has proposed the model and design and supervised the entire work and wrote the paper, Liang Fang has contributed to the simulation, preparation of the figures, and Jianqiang Liu and Shan Wu have contributed to the comments on the model, design, and paper.

Funding
This work was funded by the Natural Science Research Project of Anhui Educational Committee (KJ2016SD51) and Program of Study Abroad for Young Scholar sponsored by Anhui Educational Committee (gxfx201760).

Availability of data and materials
The datasets generated during and/or analyzed during the current study are not publicly available but are available from the corresponding author on reasonable request.

References

[1] QUINTEN M., LEITNER A., KRENN J.R., AUSSENEGG F.R., *Electromagnetic energy transport via linear chains of silver nanoparticles*, Optics Letters **23**(17), 1998: 1331-1333. https://doi.org/10.1364/OL.23.001331

[2] MAIER S.A., KIK P.G., ATWATER H.A., MELTZER S., HAREL E., KOEL B.E., REQUICHA A.A.G., *Local detection of electromagnetic energy transport below the diffraction limit in metal nanoparticle plasmon waveguides*, Nature Materials **2**(4), 2003: 229-232. https://doi.org/10.1038/nmat852

[3] CHARBONNEAU R., LAHOUD N., MATTIUSSI G., BERINI P., *Demonstration of integrated optics elements based on long-ranging surface plasmon polaritons*, Optics Express **13**(3), 2005: 977-984. https://doi.org/10.1364/OPEX.13.000977

[4] BERINI P., *Long-range surface plasmon polaritons*, Advances in Optics and Photonics **1**(3), 2009: 484-588. https://doi.org/10.1364/AOP.1.000484

[5] MORENO E., GARCIA-VIDAL F.J., RODRIGO S.G., MARTIN-MORENO L., BOZHEVOLNYI S.I., *Channel plasmon-polaritons: Modal shape, dispersion, and losses*, Optics Letters **31**(23), 2006: 3447-3449. https://doi.org/10.1364/OL.31.003447

[6] YAN M., QIU M., *Guided plasmon polariton at 2D metal corners*, Journal of the Optical Society of America B **24**(9), 2007: 2333-2342. https://doi.org/10.1364/JOSAB.24.002333

[7] NOVIKOV I.V., MARADUDIN A.A., *Channel polaritons*, Physical Review B **66**(3), 2002: 035403. https://doi.org/10.1103/PhysRevB.66.035403

[8] PILE D.F.P., GRAMOTNEV D.K., *Channel plasmon–polariton in a triangular groove on a metal surface*, Optics Letters **29**(10), 2004: 1069-1071. https://doi.org/10.1364/OL.29.001069

[9] GRAMOTNEV D.K., PILE D.F.P., *Single-mode subwavelength waveguide with channel plasmon-polaritons in triangular grooves on a metal surface*, Applied Physics Letters **85**(26), 2004: 6323-6325. https://doi.org/10.1063/1.1839283

[10] BOZHEVOLYNI S.I., VOLKOV V.S., DEVAUX E., EBBESEN T.W., *Channel plasmon-polariton guiding by subwavelength metal grooves*, Physical Review Letters **95**(4), 2005: 046802. https://doi.org/10.1103/PhysRevLett.95.046802

[11] BOARDMAN A.D., AERS G.C. TESHIMA R., *Retarded edge modes of a parabolic wedge*, Physical Review B **24**(10), 1981: 5703-5712. https://doi.org/10.1103/PhysRevB.24.5703

[12] PILE D.F.P., OGAWA T., GRAMOTNEV D.K., OKAMOTO T., HARAGUCHI M., FUKUI M., MATSUO S., *Theoretical and experimental investigation of strongly localized plasmons on triangular metal wedges for subwavelength waveguiding*, Applied Physics Letters **87**(6), 2005: 061106. https://doi.org/10.1063/1.1991990

[13] BOLTASSEVA A., VOLKOV V.S., NIELSEN R.B., MORENO E., RODRIGO S.G., BOZHEVOLNYI S.I., *Triangular metal wedges for subwavelength plasmon–polariton guiding at telecom wavelengths*, Optics Express **16**(8), 2008: 5252-5260. https://doi.org/10.1364/OE.16.005252

[14] Steinberger B., Hohenau A., Ditlbacher H., Stepanov A.L., Drezet A., Aussenegg F.R., Leitner A., Krenn J.R., *Dielectric stripes on gold as surface plasmon waveguides*, Applied Physics Letters **88**(9), 2006: 094104. https://doi.org/10.1063/1.2180448

[15] Chen Z., Holmgaard T., Bozhevolnyi S.I., Krasavin A.V., Zayats A.V., Markey L., Dereux A., *Wavelength-selective directional coupling with dielectric-loaded plasmonic waveguides*, Optics Letters **34**(3), 2009: 310-312. https://doi.org/10.1364/OL.34.000310

[16] Oulton R.F., Sorger V.J., Genov D.A., Pile D.F.P., Zhang X., *A hybrid plasmonic waveguide for subwavelength confinement and long-range propagation*, Nature Photonics **2**(8), 2008: 496-500. https://doi.org/10.1038/nphoton.2008.131

[17] Dai D.X., He S.L., *A silicon-based hybrid plasmonic waveguide with a metal cap for a nano-scale light confinement*, Optics Express **17**(19), 2009: 16646-16653. https://doi.org/10.1364/OE.17.016646

[18] Fujii M., Leuthold J., Freude W., *Dispersion relation and loss of subwavelength confined mode of metal-dielectric-gap optical waveguides*, IEEE Photonics Technology Letters **21**(6), 2009: 362-364. https://doi.org/10.1109/LPT.2008.2011995

[19] Dionne J.A., Sweatlock L.A., Atwater H.A., Polman A., *Plasmon slot waveguides: Towards chip-scale propagation with subwavelength-scale localization*, Physical Review B **73**(3), 2006: 035407. https://doi.org/10.1103/PhysRevB.73.035407

[20] Veronis G., Fan S., *Bends and splitters in metal-dielectric-metal subwavelength plasmonic waveguides*, Applied Physics Letters **87**(13), 2005: 131102. https://doi.org/10.1063/1.2056594

[21] Matsuzaki Y., Okamoto T., Haraguchi M., Fukui M., Nakagaki M., *Characteristics of gap plasmon waveguide with stub structures*, Optics Express **16**(21), 2008: 16314-16325. https://doi.org/10.1364/OE.16.016314

[22] Chen J., Li Z., Li J., Gong Q., *Compact and high-resolution plasmonic wavelength demultiplexers based on Fano interference*, Optics Express **19**(10), 2011: 9976-9985. https://doi.org/10.1364/OE.19.009976

[23] Rakhshani M.R., Mansouri-Birjandi M.A., *Dual wavelength demultiplexer based on metal–insulator–metal plasmonic circular ring resonators*, Journal of Modern Optics **63**(11) 2016: 1078-1086. https://doi.org/10.1080/09500340.2015.1125962

[24] Kamada S., Okamoto T., El-Zohary S.E., Haraguchi M., *Design optimization and fabrication of Mach-Zehnder interferometer based on MIM plasmonic waveguides*, Optics Express **24**(15), 2016: 16224-16231. https://doi.org/10.1364/OE.24.016224

[25] Haffner C., Heni W., Fedoryshyn Y., Niegemann J., Melikyan A., Elder D. L., Baeuerle B., Salamin Y., Josten A., Koch U., Hoessbacher C., Ducry F., Juchli L., Emboras A., Hillerkuss D., Kohl M., Dalton L. R., Hafner C., Leuthold J., *All-plasmonic Mach–Zehnder modulator enabling optical high-speed communication at the microscale*, Nature Photonics **9**(8), 2015: 525-528. https://doi.org/10.1038/nphoton.2015.127

[26] Pu M.B., Yao N., Hu C.G., Xin X.C., Zhao Z.Y., Wang C.T., Luo X.G., *Directional coupler and nonlinear Mach-Zehnder interferometer based on metal-insulator-metal plasmonic waveguide*, Optics Express **18**(20), 2010: 21030-21037. https://doi.org/10.1364/OE.18.021030

[27] Shin H., Fan S., *All-angle negative refraction for surface plasmon waves using a metal-dielectric-metal structure*, Physical Review Letters **96**(7), 2006: 073907. https://doi.org/10.1103/PhysRevLett.96.073907

[28] Park J., Kim KY., Lee IM., Na H., Lee SY., Lee B., *Trapping light in plasmonic waveguides*, Optics Express **18**(2), 2010: 598-623. https://doi.org/10.1364/OE.18.000598

[29] Jang M.S., Atwater H., *Plasmonic rainbow trapping structures for light localization and spectrum splitting*, Physical Review Letters **107**(20), 2011: 207401. https://doi.org/10.1103/PhysRevLett.107.207401

[30] Hu H.F., Ji D.X., Zeng X., Liu K., Gan Q.Q., *Rainbow trapping in hyperbolic metamaterial waveguide*, Scientific Reports **3**, 2013: 1249. https://doi.org/10.1038/srep01249

[31] Li D.C., Du K., Liang S.H., Zhang W.D., Mei T., *Wide band dispersionless slow light in hetero-MIM plasmonic waveguide*, Optics Express **24**(20), 2016: 22432-22437. https://doi.org/10.1364/OE.24.022432

[32] Wang B., Wang G.P., *Plasmon Bragg reflectors and nanocavities on flat metallic surfaces*, Applied Physics Letters **87**(1), 2005: 013107. https://doi.org/10.1063/1.1954880

[33] HOSSEINI A., MASSOUD Y., *A low-loss metal-insulator-metal plasmonic Bragg reflector*, Optics Express **14**(23), 2006: 11318-11323. https://doi.org/10.1364/OE.14.011318
[34] HAN Z., FORSBERG E., HE S., *Surface plasmon Bragg gratings formed in metal-insulator-metal waveguides*, IEEE Photonics Technology Letters **19**(2), 2007: 91-93. https://doi.org/10.1109/LPT.2006.889036
[35] HOSSEINI A., MASSOUD Y., *Subwavelength plasmonic Bragg reflector structures for on-chip optoelectronic applications*, [In] *2007 IEEE International Symposium on Circuits and Systems (ISCAS)*, New Orleans, LA, USA, 2007: 2283-2286. https://doi.org/10.1109/ISCAS.2007.378843
[36] LIU J.Q., WANG L.L., HE M.D., HUANG W.Q., WANG D.Y., ZOU B.S., WEN S.C., *A wide bandgap plasmonic Bragg reflector*, Optics Express **16**(7), 2008: 4888-4894. https://doi.org/10.1364/OE.16.004888
[37] CHEN S., LIU J.Q., LU H.Y., WANG Q.J., ZHU Y.Y., *Strong coupling effects between a meta-atom and MIM nanocavity*, AIP Advances **2**(3), 2012: 032186. https://doi.org/10.1063/1.4757120
[38] CHEN S., LU H.Y., LIU J.Q., ZHU Y.Y., *Strong coupling of a meta-diatom to a plasmonic nanocavity*, Chinese Physics Letters **30**(8), 2013: 087301. https://doi.org/10.1088/0256-307X/30/8/087301
[39] CHEN S., LIU J.Q., LU H.Y., ZHU Y.Y., *All-optical strong coupling switches based on a coupled meta-atom and MIM nanocavity configuration*, Plasmonics **8**(3), 2013: 1439-1444. https://doi.org/10.1007/s11468-013-9557-3
[40] HAN Z., VAN V., HERMAN W.N., HO P.-T., *Aperture-coupled MIM plasmonic ring resonators with sub-diffraction modal volumes*, Optics Express **17**(15), 2009: 12678-12684. https://doi.org/10.1364/OE.17.012678
[41] LIU Z.Y., ZHANG X.X., MAO Y.W., ZHU Y.Y., YANG Z.Y., CHAN C.T., SHENG P., *Locally resonant sonic materials*, Science **289**(5485), 2000: 1734-1736. https://doi.org/10.1126/science.289.5485.1734

Received September 24, 2023
in revised form October 30, 2023